Supplement of Atmos. Chem. Phys., 21, 5635–5653, 2021
https://doi.org/10.5194/acp-21-5635-2021-supplement

Atmospheric Chemistry and Physics
Open Access
EGU

Supplement of

Where there is smoke there is mercury: Assessing boreal forest fire mercury emissions using aircraft and highlighting uncertainties associated with upscaling emissions estimates

David S. McLagan et al.

Correspondence to: Alexandra Steffen (alexandra.steffen@canada.ca)

Contents

SECTION S1: Map of burned area.

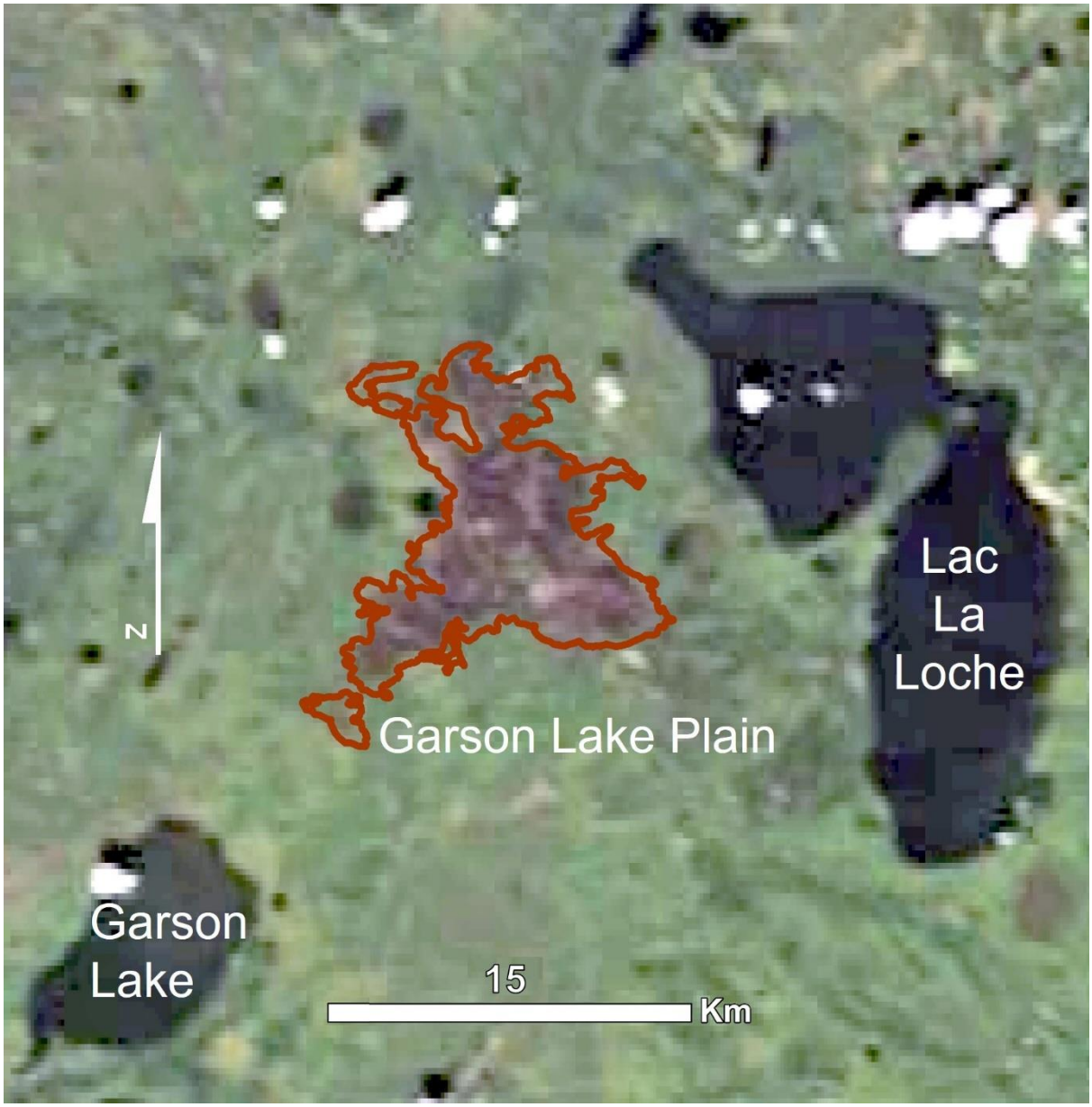

Figure S1.1: Satellite image of area burned during the fire (red polygon). Image from 14th of July 2018 – satellite image from previous days showed excessive cloud cover (NASA, 2019). Burned area of ≈88.0 km^2 was calculated from the displayed polygon using ArcGIS (ESRI) and © Google Earth Pro (Google). We assume a 10% uncertainty on this estimate.

SECTION S2: Meteorology and fire danger determinants for Lac La Loche Weather Station

Table S2.1: Mean hourly meteorology measured at Lac La Loche weather station during and preceding the monitoring flight. Preceding data are in grey and not included in summary statistics (ECCC, 2019).

date - time - timezone	wind direction	wind speed (m s^{-1})	relative humidity (%)	temperature (°C)
Mean during flight		**4.1**	**58**	**25.8**
S.D. during flight		**2.0**	**12**	**2.0**
2018-06-25 13:00:00 CST	SE	6.4	46	27.9
2018-06-25 12:00:00 CST	SE	6.1	46	27.2
2018-06-25 11:00:00 CST	SE	2.5	59	26.3
2018-06-25 10:00:00 CST	SSE	3.1	66	24.8
2018-06-25 09:00:00 CST	SSE	2.2	73	23.0
2018-06-25 08:00:00 CST	SSE	2.8	82	20.8
2018-06-25 07:00:00 CST	S	2.8	90	18.7
2018-06-25 06:00:00 CST	S	3.3	93	17.4
2018-06-25 05:00:00 CST	S	3.1	95	16.6
2018-06-25 04:00:00 CST	SSW	3.1	94	17.2
2018-06-25 03:00:00 CST	S	2.8	92	17.7
2018-06-25 02:00:00 CST	S	2.8	89	18.3
2018-06-25 01:00:00 CST	SSW	2.8	85	19.5
2018-06-25 00:00:00 CST	SSW	2.5	83	20.2

Note Central Standard Time (CST) is the same as Mountain Daylight Time (MDT)

Table S2.2: Mean daily meteorology measured at Lac La Loche weather station for the day of the monitoring flight and the preceding week (ECCC, 2019). Colours represent the severity of conditions: green – good; yellow – okay; red – bad; dark red – very bad.

Date	Wind Speed (m s^{-1})	Wind Dir	Temp (°C)	RH (%)	Rain (24 hr)	Fine Fuel Moisture code FFMC	duff moisture code DMC	sheltered duff moisture code SDMC	drought code DC	Initial Spread Index ISI	Build up index BUI	Fire Weather Index FWI
25/06/2018	2.9	SE	23.4	67.0	0	90.9	57.5	113.0	361.4	8.2	82.3	25.0
24/06/2018	2.5	SSW	20.7	73.1	0	88.8	52.6	106.1	352.7	5.7	76.6	18.5
23/06/2018	3	ESE	20.9	69.7	0	88.7	49.4	101.7	344.5	6.1	72.7	18.9
22/06/2018	1.4	SE	22.1	66.5	0	87.2	45.5	96.5	336.4	3.7	68.0	12.5
21/06/2018	1.7	SW	23.5	54.9	0	91.8	43.6	93.8	328.9	7.5	65.5	20.9
20/06/2018	1.7	SW	26.4	47.1	0	93.5	39.2	87.8	320.3	9.5	60.0	23.6
19/06/2018	1.4	SSW	24.3	44.5	0	92.8	32.9	79.1	311.1	8.2	52.1	19.8
18/06/2018	1.7	SSW	23.1	41.8	0	92.6	27.2	71.3	302.3	8.4	44.4	18.4

SECTION S3: Determination of GEM as the sampled analyte of the in-flight Tekran 2537X system.

The atmospheric Hg species measured in these flights has been determined to be GEM. A number of factors contributed to this conclusion. The soda-lime trap and quartz wool plugs at either end of the soda-lime material are expected to remove the majority (if not all) GOM from the sampled air (Lyman and Jaffe, 2012; Gustin et al., 2013; Slemr et al., 2016; 2018). A portion of GOM has also been suggested to sorb to the Teflon filter (≈10 – 50 %; Stupple et al., 2019) and unheated Teflon sampling lines (Finley et al., 2013; Gustin et al., 2015). It has been reported that GOM can "bleed-off" from some system components during sampling, which has the potential to cause a slight increase in the GEM signal, especially in elevated relative humidity and O_3 mixing ratios (Slemr et al., 2016; Lyman and Jaffe 2012). Nonetheless, we expect this to be minimal because (i) the system remained on and was continuously flushed with "zero" air before the flight (this was not the case when "bleed-off" was observed in Slemr et al., 2016), (ii) the minor losses (≈6 – 20 % of sampled GOM) are described from a system employing quartz wool alone, whereas we employed both quartz wool and soda-lime (Lyman and Jaffe 2012), (iii), as previously mentioned, GOM has not been previously detected to be elevated in wildfire biomass burning plumes, and (iv) relative humidity during this flight was not elevated (34 – 58 %).

GEM as the species sampled by this system was confirmed during another flight in Environment and Climate Change Canada's Oil Sands Monitoring Program on May 31st, 2018. This flight was an emissions box flight (circumnavigation of an oil sands facility at increasing height above the ground to assess the extent of pollutant emissions) of the CNRL Horizon facility. During this flight an alternating sampling system (alternating every four samples) was employed to draw sample air through the two different particle filter systems: (i) regular 0.25 µm Teflon filter and (ii) a 0.4 µm polysulphone cation exchange membrane (CEM) filter. The latter has been shown to remove both GOM and PBM yet allows GEM to pass at an efficiency of >99.9 % under elevated GEM conditions (Miller et al., 2019). There was no significant difference between the mean concentration determined using the CEM filter (1.08 ng m^{-3}) and the regular Teflon filter (1.08 ng m^{-3}) across all samples during the flight (p = 0.921; Figure S3-1). There was evidence of minor primary GEM emissions during this flight (significant positive correlation with black carbon; $p < 0.05$; Figure S3-2). Evidence of primary GEM emissions was also observed on another flight around the same facility (significant positive correlation with black carbon; $p < 0.05$), supporting the notion that the different sampling methodologies did not alter the results even in the presence of Hg emissions. We do expect there to be GOM emissions from these facilities if there are GEM emissions, typical for industrial combustion emissions (Carpi, 1997). Additionally, an Environment and Climate Change Canada ground

monitoring station in the centre of the oil sands facilities measured GOM concentrations of up to 280 pg m^{-3} on April 4th, 2018 when the monitoring station was downwind from CNRL Horizon and other adjacent facilities.

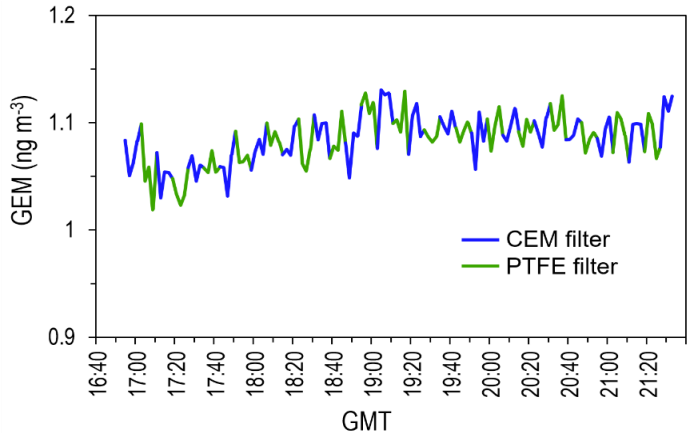

Figure S3.1: Gaseous oxidised mercury (GEM) concentration measured during deployment of alternating Teflon and cation exchange membrane filters during an emissions box flight around CNRL Horizon, Suncor Fort Hills, and Syncrude Aurora mining facilities on May 31st, 2018. The flight employed an alternating inlet system that changed sampling lines every four samples. The first inlet setup used a 0.4 µm polysulphone, cation exchange membrane (CEM) shown to sorb gaseous oxidised mercury (GOM) and particulate bound mercury (PBM), while allowing GEM to pass through the membrane at >99.9% efficiency (Miller et al., 2019). The second inlet setup utilised the standard Tekran issued 0.25 µm Teflon filter.

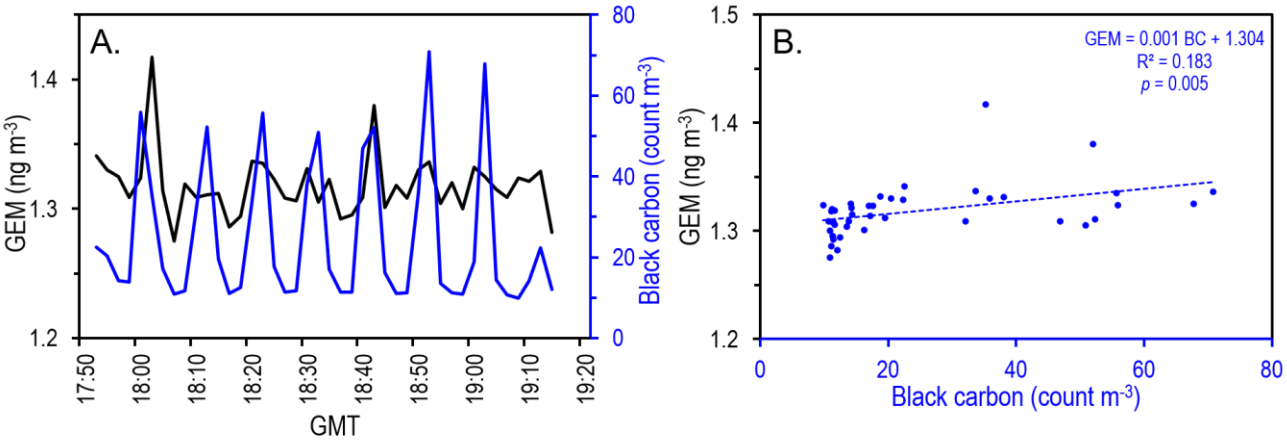

Figure S3.2: Evidence of primary GEM emissions from another emissions box flight on 10th of April, 2018 around the CNRL Horizon facility given by the significant, positive relationship between black carbon (primary pollutant) and GEM.

SECTION S4: Regressions of GEM against other primary pollutants across whole flight.

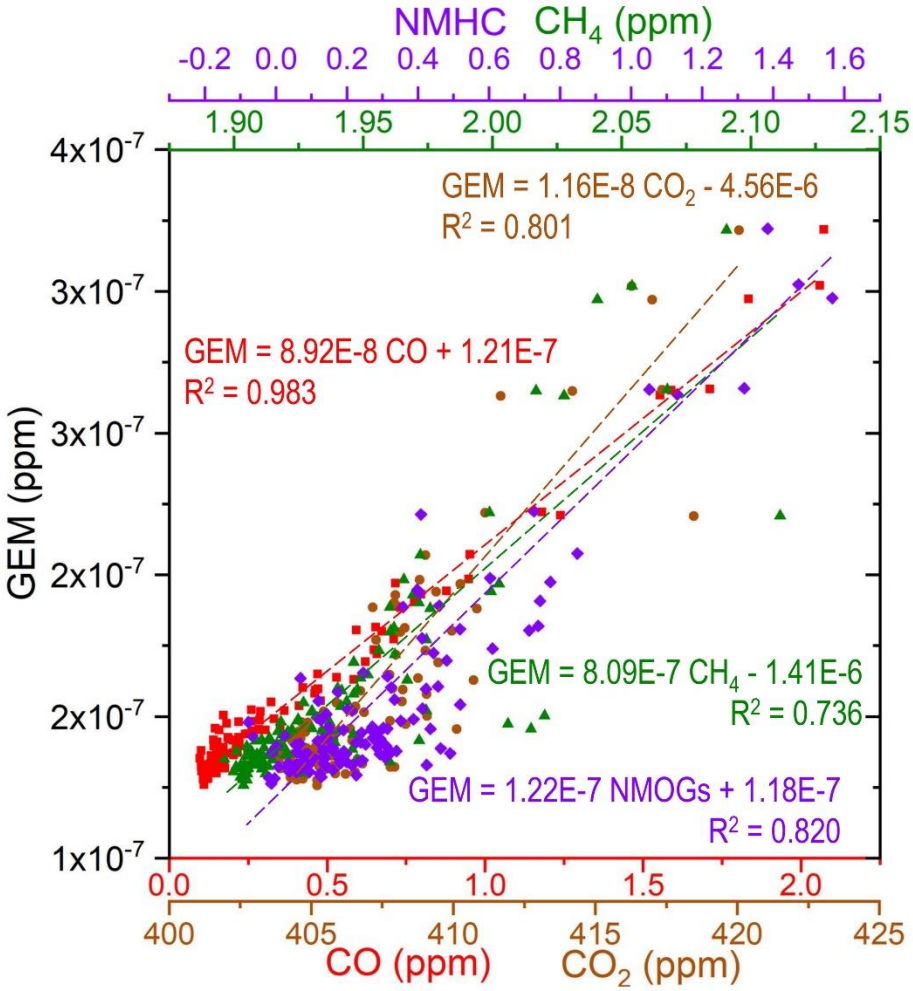

Figure S4.1: Mixing ratio regressions of GEM against CO, CO_2, and CH_4 for data from the whole flight (n = 120); ERs of GEM and each of the pollutants are derived from the slopes of these regressions. ERs for the whole flight data are as follows – GEM:CO = (8.92 ± 0.11) x 10^{-8}; GEM:CO_2 = (1.07 ± 0.05) x 10^{-8}; GEM:CH_4 = (7.53 ± 0.41) x 10^{-7}; GEM:NMOG = (1.09 ± 0.05) x 10^{-7}. These values are within 5 % of the ERs derived from only the GEM data elevated >1.25x background concentration. These regressions include data measured outside the fire plume; hence, data with elevated pollutant concentrations are preferred. See "cut-off" sensitivity analysis in Section S5 for details.

SECTION S5: Sensitivity analysis of "cut-off" value for the determination of elevated concentrations.

Table S5.1: Sensitivity analysis of "cut-off" value for the determination of elevated concentrations. Blue text marks highest R^2 value for each reference compound. Red text marks data sets with reference compound mixing ratios below their respective background mixing ratio value.

GEM cut-off fraction	1.1x background GEM conc.			1.25x background GEM conc.			1.5x background GEM conc.		
GEM cut-off conc. (ng m^{-3})	1.29			1.47			1.76		
qualified data (*n*)	50			24			10		
Reference compound	ER Estimate & S.E.	R^2	values < BG	ER Estimate & S.E.	R^2	values < BG	ER Estimate & S.E.	R^2	values < BG
CO	(8.88 ± 0.19) * 10^{-8}	0.978	0	(9.29 ± 0.29) * 10^{-8}	0.979	0	(1.01 ± 0.06) * 10^{-7}	0.970	0
CO_2	(1.07 ± 0.09) * 10^{-8}	0.765	6	(1.03 ± 0.13) * 10^{-8}	0.750	0	(9.23 ± 2.64) * 10^{-9}	0.528	0
CH_4	(8.91 ± 0.87) * 10^{-7}	0.634	0	(9.17 ± 1.22) * 10^{-7}	0.671	0	(6.34 ± 2.63) * 10^{-7}	0.321	0
NMOGs	(1.21 ± 0.07) * 10^{-7}	0.834	2	(1.24 ± 0.12) * 10^{-7}	0.814	0	(1.10 ± 0.18) * 10^{-7}	0.795	0

Using an elevated GEM concentration "cut-off" value of 1.1x background results in the most data that can be included in emissions ratios (ERs), emissions factors (EFs) and emissions estimate calculations (n = 50). However, for both CO and CH_4 the highest R^2 value of regressions with GEM are when the elevated GEM concentration "cut-off" value is 1.25x background. While the R^2 of the regressions of GEM against both CO_2 and NMOGs were higher for the 1.1x background "cut-off", both data sets included reference compound mixing ratios that were less than the determined background values (six and two, respectively). Increasing the "cut-off" value to 1.5x background, reduced the data sets to only 10 values and resulted in poorer fitting regressions (lower R^2 values) for all reference compounds. Thus, we deem the "cut-off" value of 1.25x background to be the most appropriate to determine elevated concentrations based on these data.

SECTION S6: Emissions estimates for carbon monoxide, carbon dioxide, and methane derived from the literature.

Table S6.1: Emissions estimates of reference contaminants carbon monoxide (CO), carbon dioxide (CO_2), and methane (CH_4) from literature.

Estimated global emissions (Tg yr^{-1})			
Reference contaminant	CO[a]	CO_2[b]	CH_4[c]
estimate	318	7570	12.9
uncertainty	91	1400	3.3
Estimated boreal forest emissions (Tg yr^{-1})			
Reference contaminant	CO[a]	CO_2[b]	CH_4[c]
estimate	29	620	1.11
uncertainty	23	480	0.87

a) Mean of four methods used by Jiang (2017) for 2001 – 2015. Uncertainty terms were based on the standard deviation of the yearly CO emissions for each method.

b) Mean of four methods used by Shi and Matsunaga (2017) for 2002 – 2011. The values used for these estimates were taken from Figure 2 of that paper using PlotDigitizer v2.6.8 (Huwaldt and Steinhorst, 2015). Uncertainty terms were taken from Table S2 in the supporting information.

c) Mean of top-up and bottom-down methods used by Worden et al. (2017) for 2001 – 2015. Boreal forest estimates were not available for CH_4 emissions. The mean of the ratios of boreal-to-global emissions for CO and CO_2 was used, as well as the mean coefficient of variation of their uncertainty terms. The estimate and uncertainty terms for the global CH_4 emissions were then adjusted according to this calculated boreal-to-global ratio.

SECTION S7: Calculated emissions factors used in determination of Hg emissions from biomass burning.

Emissions factors for CO, CO2, and CH4 in boreal forests from the literature were 121 ± 47, 1530 ± 140, and 5.5 ± 2.5 g kg^{-1}, respectively (Andreae, 2019). These values were used in the calculation of the emissions factors for emissions estimate method 2 (EEM2) listed in Table S7.1 below. The emissions factors for emissions estimate method 3 (EEM3) were calculated using the measured ΔGEM, ΔCO, ΔCO_2, and ΔCH_4 concentration measured during the monitoring flight of the Garson Plains fires.

Table S7.1: Calculated emissions factors (EFs) in µg kg^{-1} used in the determination of emissions estimate method 2 (EEM2) and emissions estimate method 3 (EEM3). The uncertainty terms for EEM3 emissions factors include the standard deviation of the background concentrations used for GEM, CO, CO_2, and CH_4.

	EFs used for EEM2						**EFs used for EEM3**		**EFs used for EEM3 – 90:10 CO2:CO ratio***	
Reference contaminant	CO (39%)		CO_2 (10%)		CH_4 (46%)		N/A (28%)		N/A (11%)	
Hg Scenario	estimate	±	estimate	±	estimate	±	estimate	±^	estimate	±^
0% PBM	80	31	71.7	11.0	63	30	99	26	77.0	8.5
3.8% PBM	84	33	74.5	11.4	66	31	103	27	80.1	8.8
15% PBM	95	37	84.3	12.9	74	35	117	31	90.6	10.0
30% PBM	115	45	102	16	90	43	141	37	110	12.1

Values in parenthesis next to reference contaminants are the coefficient of variation % (CV%) for that set of estimates.

N/A – not applicable.

± Denotes uncertainty term.

^ The uncertainty terms for EEM3 emissions factors include the standard deviation of the mean value used to calculate the background concentrations used for GEM, CO, CO_2, and CH_4.

* Another set of emissions factors were also calculated for EEM3 using the assumption from Friedli et al. (2003b) of a 90:10 CO2:CO ratio (assumes 0 % CH_4 and 0 % C_{other}), which was calculated by multiplying the measured CO concentrations by 10 (they did not measure CO_2). The uncertainty of this estimate does not include any uncertainty associated with the assuming the other measured carbon contaminants from CO. All values include one extra significant digit to reduce rounding errors for any subsequent calculations.

SECTION S8: Active fires detected by MODIS Satellites.

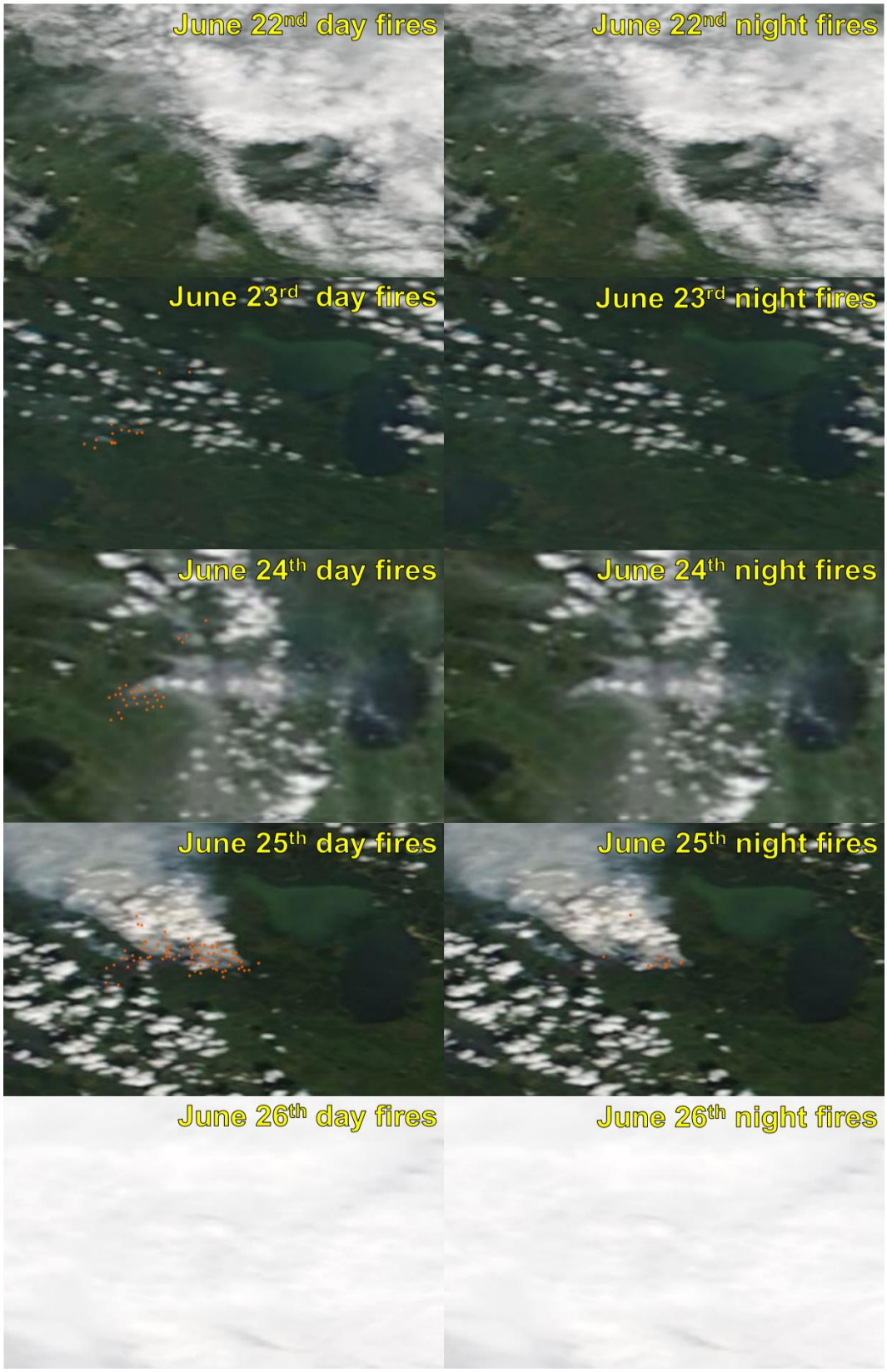

Figure S8.1: Active fire and thermal anomalies detected both day and night by the Aqua MODIS and Terra MODIS satellites (NASA, 2019).

Table S8.1: The number of fire and thermal anomalies derived from the Aqua MODIS and Terra MODIS satellites as displayed in Fig. S8.1

Period	Fire & Thermal anomalies	Uncertainty*
June 22nd day	0	0
June 22nd night	0	0
June 23rd day	16	4.3
June 23rd night	0	0
June 24th day	29	7.7
June 24th night	0	0
June 25th day	83	22
June 25th night	13	3.5
June 26th day	0	0
June 26th night	0	0

* Uncertainty of 26.6 % of MODIS Fire and thermal anomalies as determined by (Freeborn et al., 2014)

REFERENCES:

Carpi, A.: Mercury from combustion sources: a review of the chemical species emitted and their transport in the atmosphere. Water Air Soil Pollut., 98, 241-254, https://doi.org/10.1023/A:1026429911010, 1997.

ECCC: Daily and hourly Climate Normals, Environment and Climate Change Canada (ECCC). Accessed: 3 September 2019. http://climate.weather.gc.ca, 2019.

Finley, B. D., Jaffe, D. A., Call, K., Lyman, S., Gustin, M. S., Peterson, C., Miller, M. and Lyman, T: Development, testing, and deployment of an air sampling manifold for spiking elemental and oxidized mercury during the Reno Atmospheric Mercury Intercomparison Experiment (RAMIX). Environ. Sci. Technol., 47, 7277-7284, https://doi.org/10.1021/es304185a, 2013.

Freeborn, P. H., Wooster, M. J., Roy, D. P., and Cochrane, M. A.: Quantification of MODIS fire radiative power (FRP) measurement uncertainty for use in satellite-based active fire characterization and biomass burning estimation. Geophys. Res. Lett., 41, 1988-1994, https://doi.org/10.1002/2013GL059086, 2014.

Gustin, M. S., Huang, J., Miller, M. B., Peterson, C., Jaffe, D. A., Ambrose, J., Finley, B. D., Lyman, S. N., Call, K., Talbot, R.,Feddersen, D., Mao, H., and Lindberg, S. E.: Do we understand what the mercury speciation instruments are actually measuring? Results of RAMIX. Environ. Sci. Technol., 47, 7295-7306, https://doi.org/10.1021/es3039104, 2013.

Gustin, M. S., Amos, H. M., Huang, J., Miller, M. B., and Heidecorn, K.: Measuring and modeling mercury in the atmosphere: a critical review. Atmospheric chemistry and physics, 15(10), 5697-5713, https://doi.org/10.5194/acp-15-5697-2015, 2015.

Jiang, Z., Worden, J. R., Worden, H., Deeter, M., Jones, D., Arellano, A. F., and Henze, D. K.: A 15-year record of CO emissions constrained by MOPITT CO observations. Atmos. Chem. Phys., 17, 4565-4583, https://doi.org/10.5194/acp-17-4565-2017, 2017.

Lyman, S. N., and Jaffe, D. A.: Formation and fate of oxidized mercury in the upper troposphere and lower stratosphere. Nat. Geosci., 5, 114-117, https://doi.org/10.1038/ngeo1353, 2012.

Miller, M. B., Dunham-Cheatham, S. M., Gustin, M. S., and Edwards, G. C.: Evaluation of cation exchange membrane performance under exposure to high Hg^0 and $HgBr_2$ concentrations. Atmos. Meas. Tech., 12, 1207-1217, https://doi.org/10.5194/amt-12-1207-2019, 2019.

NASA: National Aeronautics and Space Administration (NASA) Worldview: Earth Observing System Data and Information System (EOSDIS), Last accessed: 8 August 2020, https://worldview.earthdata.nasa.gov/, 2019.

Slemr, F., Weigelt, A., Ebinghaus, R., Kock, H. H., Bödewadt, J., Brenninkmeijer, C. A., Rauthe-Schöch, A., Weber, S., Hermann, M., Becker, J., Zahn, A., and Martinsson, B.: Atmospheric mercury measurements onboard the CARIBIC passenger aircraft. Atmos. Meas. Tech., 9, 2291-2302, https://doi.org/10.5194/amt-9-2291-2016, 2016.

Shi, Y., and Matsunaga, T.: Temporal comparison of global inventories of CO 2 emissions from biomass burning during 2002–2011 derived from remotely sensed data. Environ. Sci. Poll. Res., 24, 16905-16916, https://doi.org/10.1007/s11356-017-9141-z, 2017.

Stupple, G. W., McLagan, D. S., Steffen, A.: In situ reactive gaseous mercury uptake on Radiello diffusive barrier, cation exchange membrane and teflon filter membranes during atmospheric depletion events, Proceedings of the 14th International Conference on Mercury as a Global Pollutant, Krakow, Poland, 8–13 September 2019. https://mercury2019krakow.com/gb/programme/program-overview/oral-sessions.html, 2019.

Worden, J. R., Bloom, A. A., Pandey, S., Jiang, Z., Worden, H. M., Walker, T. W., Houweling, S. and Röckmann, T.: Reduced biomass burning emissions reconcile conflicting estimates of the post-2006 atmospheric methane budget. Nat. Commun., 8, 1-11, https://doi.org/10.1038/s41467-017-02246-0, 2017.